Synergistic Enhancement of Strength and Ductility in Crosslinked Polymer Binders for High-Stability Silicon Anodes in Lithium-Ion Batteries

Junho Kim†[a], Gyuri Kim†[b], Ji Young Kim[a], Sohyun Kim[a], Hyunjun Lee[b], Youngho Eom[b] In Hwan Jung*[b] and Hansu Kim*[a]

[a] Department of Energy Engineering, Hanyang University, 17 Haengdang-dong Seongdong-gu, Seoul 04763, Republic of Korea

[b] Department of Organic and Nano Engineering, and Human-Tech Convergence Program, Hanyang University, 222 Wangsimni-ro, Seongdong-gu, Seoul 04763, Republic of Korea.

*Corresponding author.

E-mail address: inhjung@hanyang.ac.kr (I.H.Jung), khansu@hanyang.ac.kr (H.Kim)

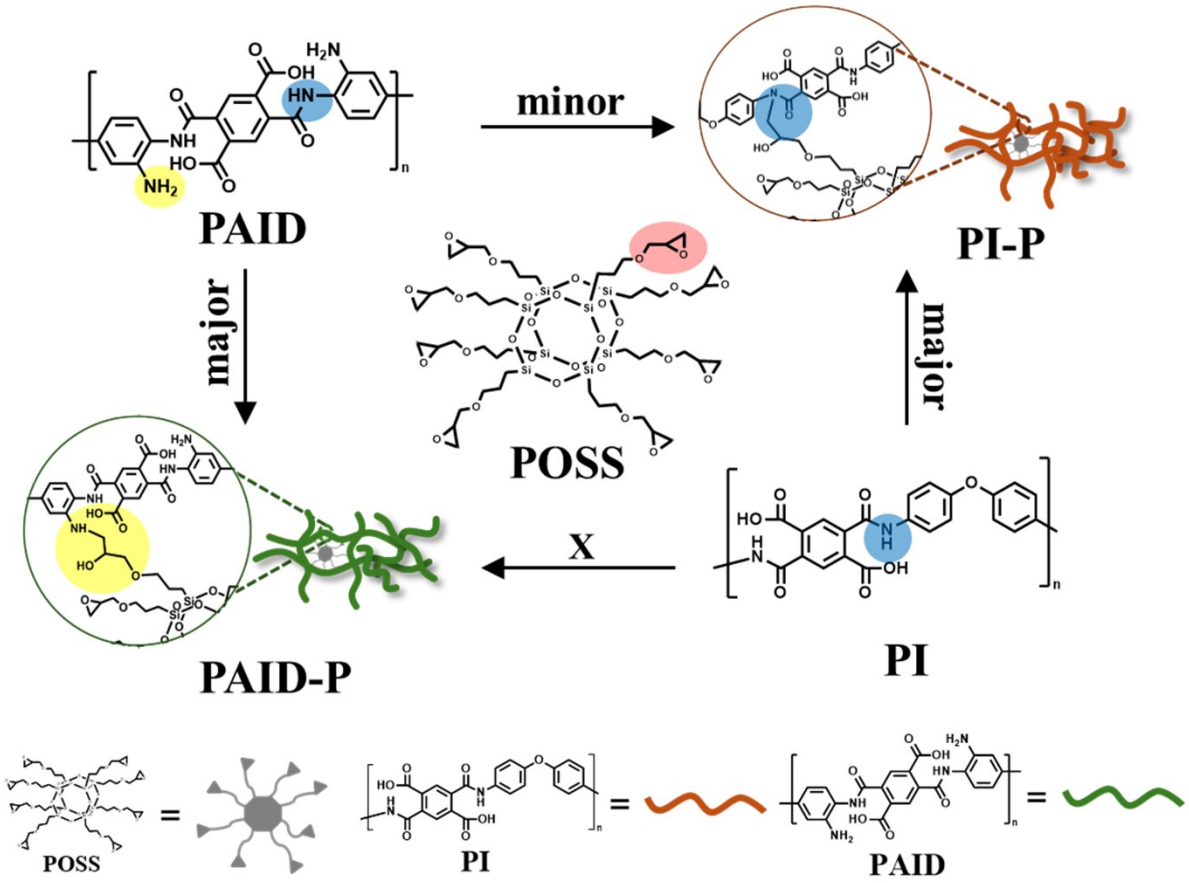

Scheme S1. Synthesis procedure and reaction mechanism of PI-P and PAID-P.

Molecular Weight Averages

Peak #	RT (min)	Mp (g/mol)	Mn (g/mol)	Mw (g/mol)	Mz (g/mol)	Mz+1 (g/mol)	PD
1	8.936	2989174	4526102	5400193	6784917	8717337	1.193122

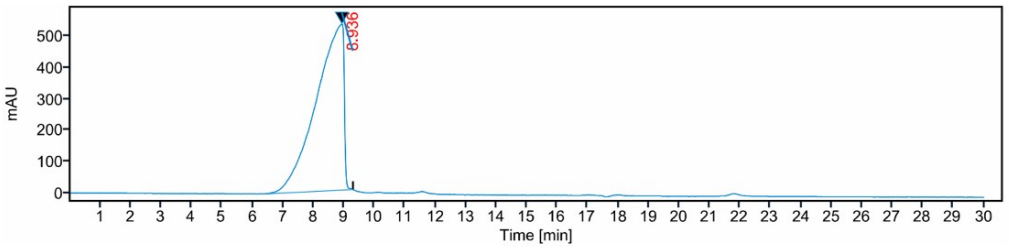

Fig. S1. Gel permeation chromatography graph of PI.

Molecular Weight Averages

Peak #	RT (min)	Mp (g/mol)	Mn (g/mol)	Mw (g/mol)	Mz (g/mol)	Mz+1 (g/mol)	PD
1	7.656	9240107	2629594	7672238	11935118	14534083	2.917651

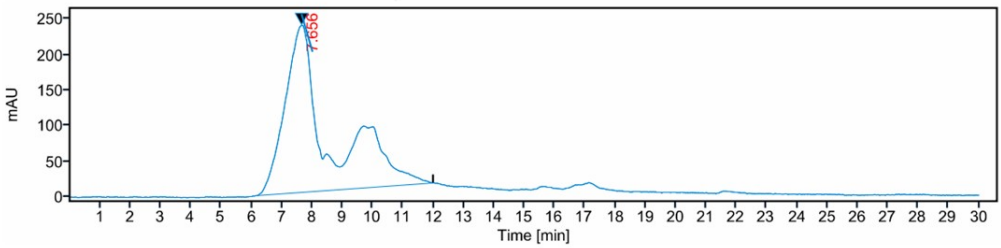

Fig. S2. Gel permeation chromatography graph of PAID.

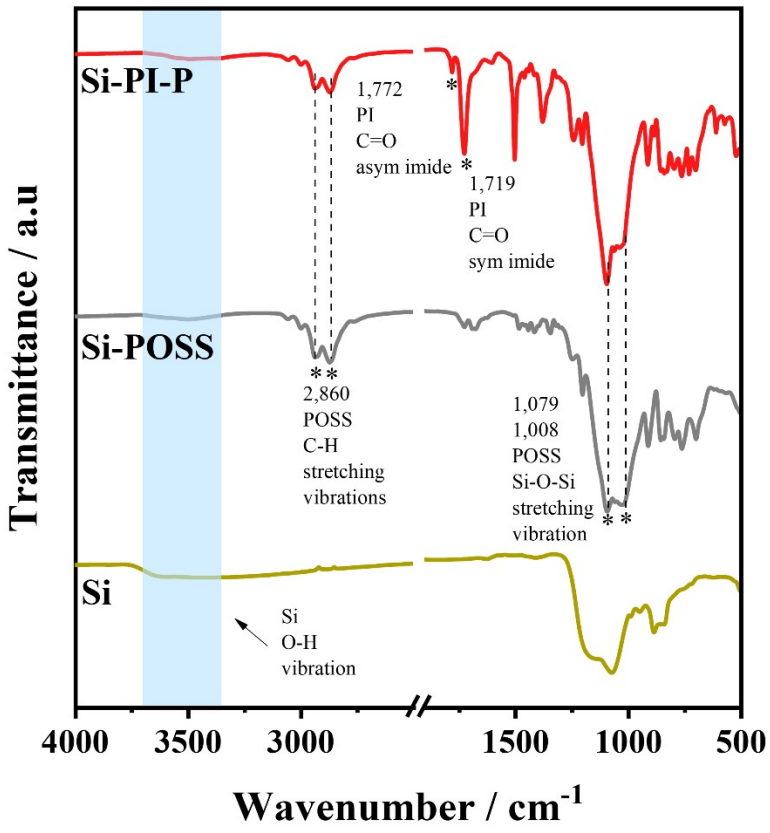

Fig. S3. FT-IR spectra of PI-P binder and POSS cross-linker with Si particles.

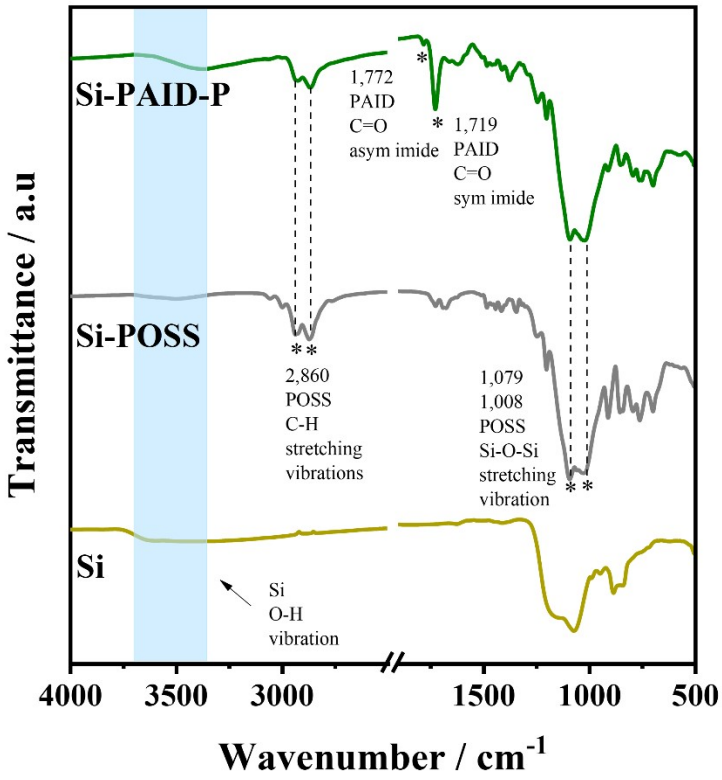

Fig. S4. FT-IR spectra of PAID-P binder and POSS cross-linker with Si particles.

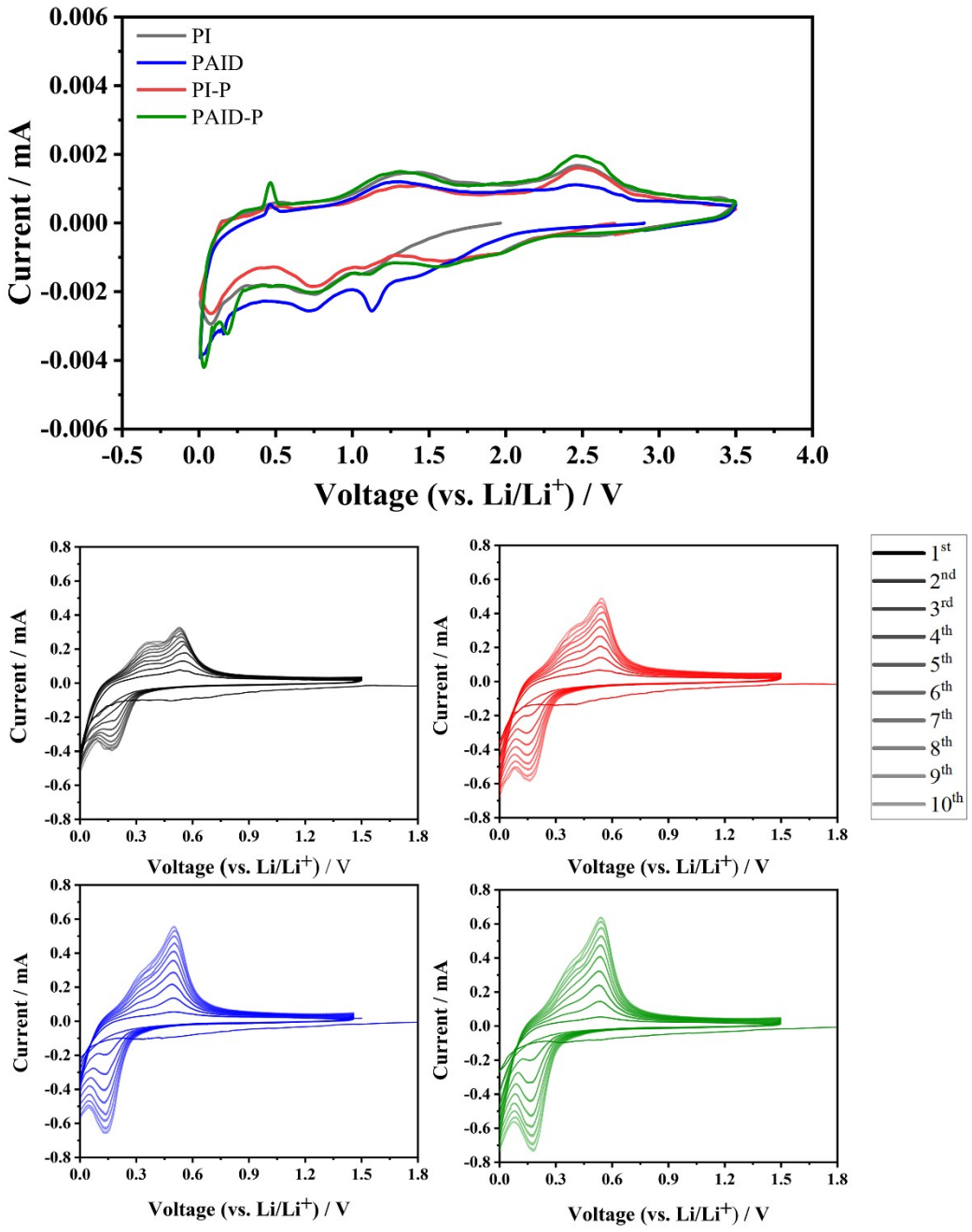

Fig. S5. Cyclic voltammogram of Si anodes with PI, PAID, PI-P, and PAID-P at a scan rate of 10 $\mu V\ s^{-1}$.

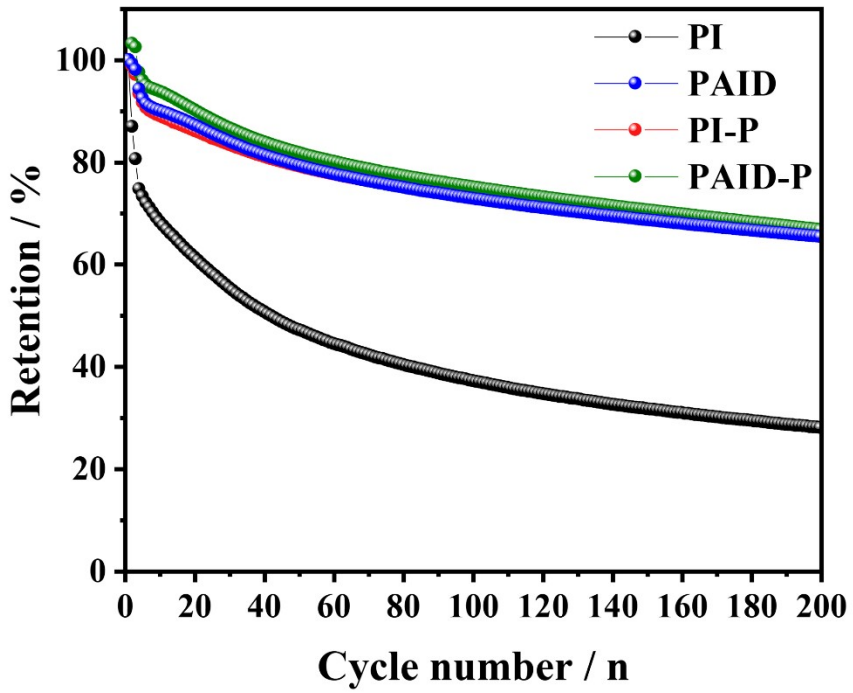

Fig. S6. Capacity retention values of Si anode depend on different binders at current density of 0.2C.

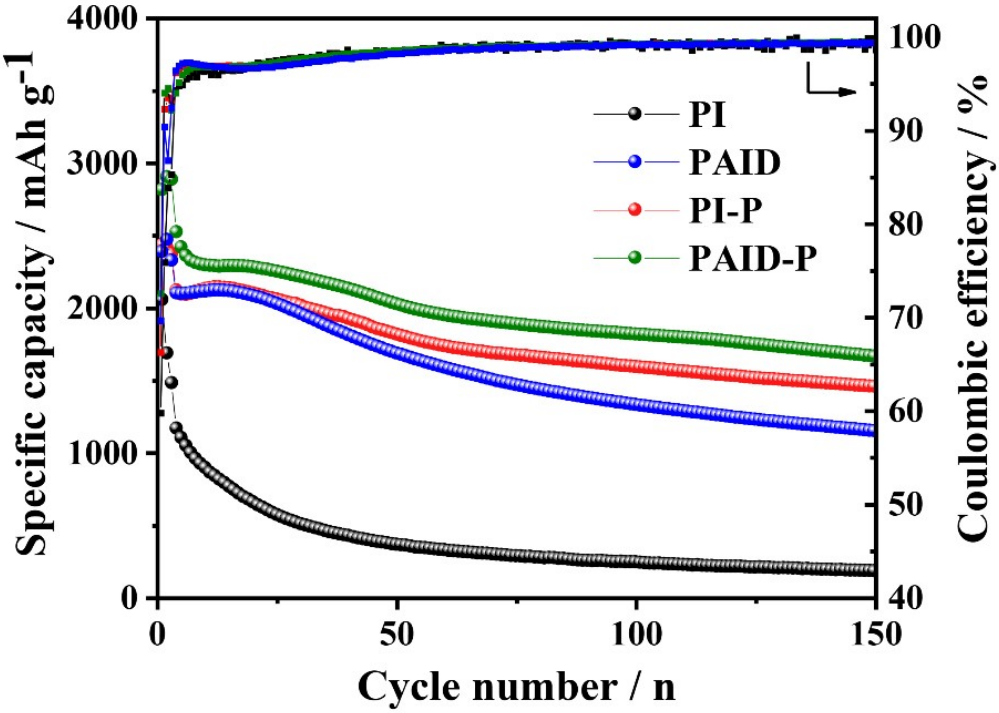

Fig. S7. Electrochemical cycle performance Si anode depends on different binders at different current density of 1C.

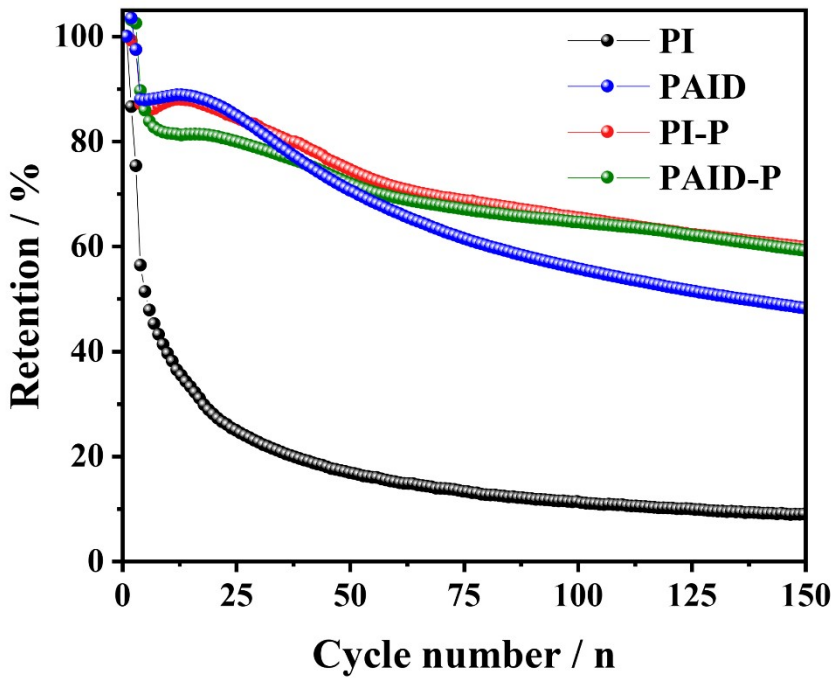

Fig. S8. Capacity retention values of Si anode depend on different binders at current density of 1C.

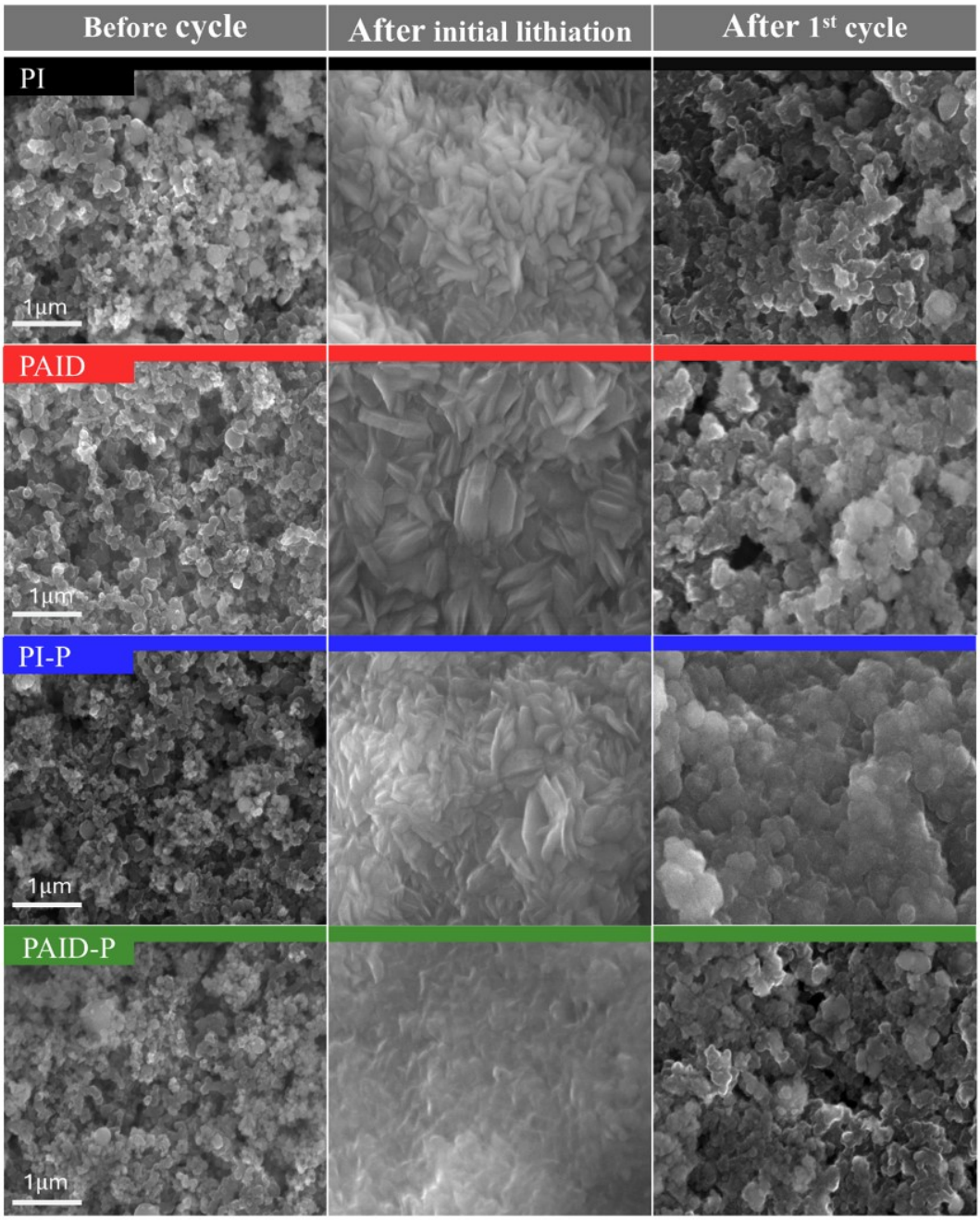

Fig. S9. Top-viewed SEM images of PI-Si anode, PAID-Si anode, PI-P-Si anode, and PAID-P-Si anode before cycling, after initial lithiation, and after 1st cycle.

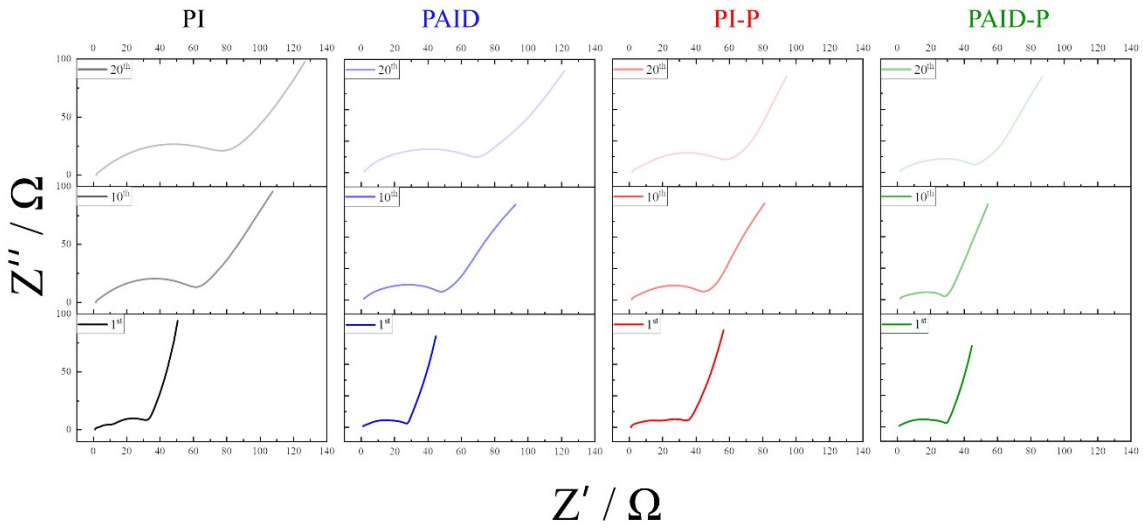

Fig. S10. Nyquist plots of Si anode depending on different polymer binders at different cycles.

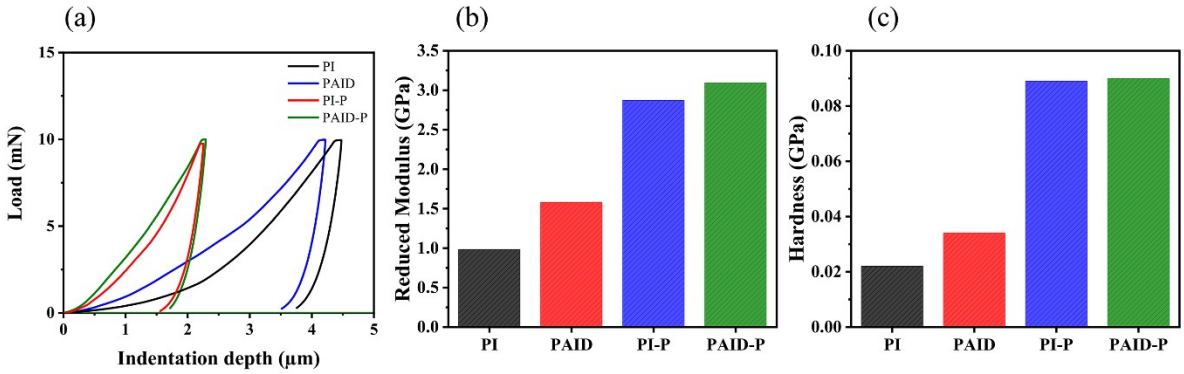

Fig. S11. (a) Nanoindentation profiles of the Si anodes with PI, PAID, PI-P, PAID-P binders. (b) Reduced modulus and (c) hardness of Si anode with different binders.

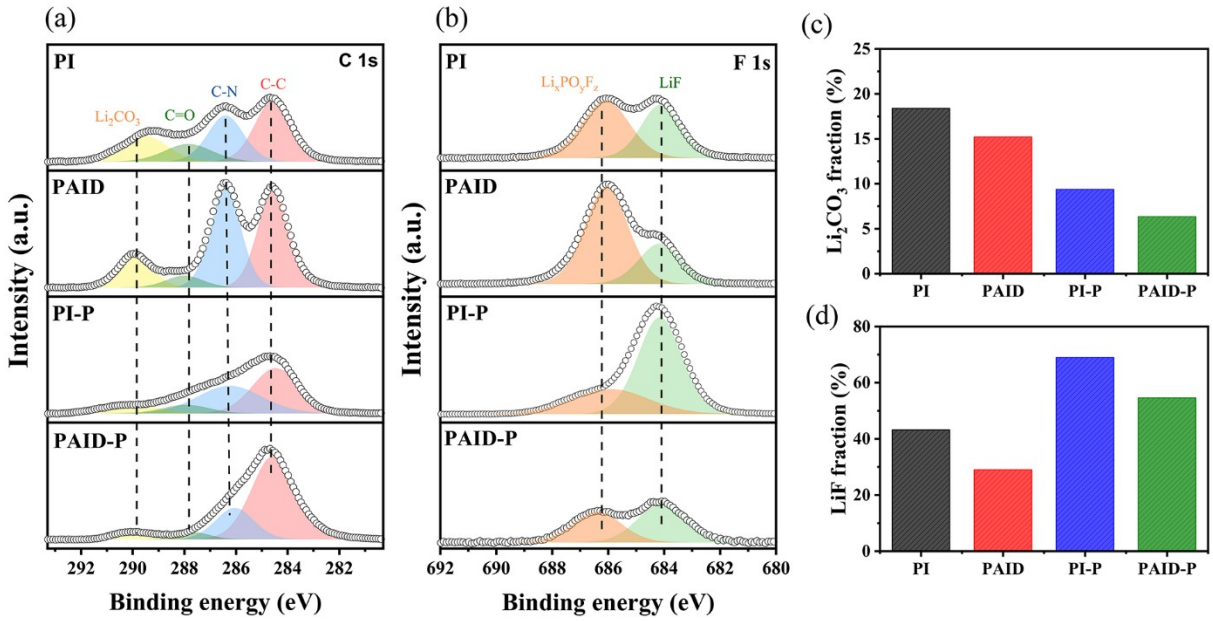

Fig. S12. XPS analysis on the SEI composite of the Si anodes with different binders. (a) C 1s, (b) F 1s spectra; (c) Li_2CO_3 fraction; and (d) LiF fraction of the cycled PI, PAID, PI-P, PAID-P Si anode after 200 cycles under 0.2C at 25°C.

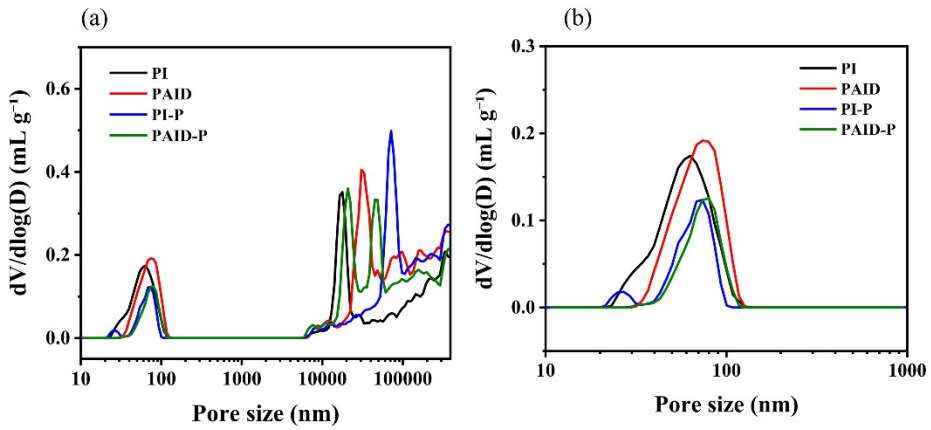

Fig. S13. Pore size distribution of Si anodes with different binders measured by mercury intrusion porosimetry. (a) Full-range pore size distribution and (b) magnified view in the small pore region, comparing PI, PAID, PI-P, and PAID-P based Si anodes.

Binder	Peel test Average force / *N*	SAICAS Average force / *N*
PI	1.1	0.10
PAID	3.9	0.16
PI-P	4.2	0.25
PAID-P	5.4	0.30

Table S1. Average force of peel test and SAICAS for composite electrodes depend on binders.

Binder	Reduced modulus(GPa)	Hardness (GPa)	Indentation depth (μm)
PI	0.983	0.022	4.44
PAID	1.58	0.034	4.18
PI-P	2.872	0.089	2.24
PAID-P	3.093	0.09	2.26

Table S2. Reduced modulus, hardness indentation depth for composite electrodes depend on binders.

		PI	PAID	PI-P	PAID-P
C 1s	C-C	60885.94	86045.84	57838.50	99205.11
	C-N	45244.46	83627.44	49083.75	32927.34
	C=O	27062.55	12286.61	11223.58	6370.76
	Li_2CO_3	30088.58	32647.89	12211.51	9383.27
	Li_2CO_3 Fraction	18.4%	15.2%	9.37%	6.34%
F 1s	LiF	74605.07	61713.19	229447.26	13553.51
	$Li_xPO_yF_z$	98172.92	150771.54	103185.07	11260.57
	LiF fraction	43.2%	29.0%	69.0%	54.6%

Table S3. XPS analysis on the SEI composite of the Si anodes with different binders.

	PI	PAID	PI-P	PAID-P
Total pore area (m^2/g)	4.519	3.712	2.056	1.733
Median pore diameter (μm)	0.05282	0.06101	0.06455	0.07163
Avg pore diameter (μm)	0.1988	0.3598	0.5151	0.6491
Porosity (%)	23.42	27.63	5.15	19.75

Table S4. Pore structure parameters of different samples obtained from mercury intrusion porosimetry

Binder	Active material	Current density	Initial discharge capacity	Cycle performance	polyimide-derivatives	Ref.
P84	SiNP (30nm)	0.2 A g^{-1}	2392 mAh g^{-1}	1313 mAh g^{-1} after 300 cycles	copolyimide	*1*
PI-COOH	SiNP (<60nm)	0.5 A g^{-1}	2557.9 mAh g^{-1}	809 mAh g^{-1} after 100 cycles	carboxyl-functionalized polyimide	*2*
NTPI-COOH	SiNP (<60nm)	0.5 A g^{-1}	2611.6 mAh g^{-1}	1252.2 mAh g^{-1} after 100 cycles	carboxyl-functionalized polyimide	*3*
API	SiNP (50nm)	2 A g−1	2695 mAh g^{-1}	1444 mAh g^{-1} after 200 cycles	Adenine-Derived Polyimide	*4*
PAID20	SiNP (100nm)	0.2 C	2663 mAh g^{-1}	1792 mAh g^{-1} after 200 cycles	copolyimide	*5*
PAID-P	SiNP (100nm)	0.2 C	2820.6 mAh g^{-1}	1881 mAh g^{-1} after 200 cycles	Crosslinking polyimide	*This work*

Table S5. Comparison of cycling performance between the PAID-P and previously reported polyimide-derivatives binders for Si anodes.

References

1. J. Choi, K. Kim, J. Jeong, K. Y. Cho, M.-H. Ryou and Y. M. Lee, Acs Appl Mater Inter, 2015, 7, 14851-14858.

2. Y. Xu, Q. Zhang, N. Lv, H. Li, Z. Wei, Y. Wang and H. Tang, Energ Fuel, 2023, 37, 2441-2448.

3. P. Du, H. Zhou, Y. Xu and Y. Wang, ACS Omega, 2026.

4. W. Tan, B. Liang, M. Chen, Z. Song, M. Yi, J. Hu, K. Zeng and G. Yang, ACS Applied Energy Materials, 2023, 6, 10723-10733.

5. J. Kim, G. Kim, Y. K. Park, G. Lim, S. T. Kim, I. H. Jung and H. Kim, Advanced Functional Materials, 2023, 33, 2303810.